(Preprint) AAS 21-451

SPACECRAFT FORMATION CONTROL NEAR A PERIODIC ORBIT USING GEOMETRIC RELATIVE COORDINATES

Ian Elliott* and Natasha Bosanac†

A feedback control law is introduced for spacecraft relative motion about a periodic orbit with an oscillatory mode in the circular restricted three-body problem. The control law feeds back errors expressed using a geometric relative coordinate set that describes a state relative to a periodic orbit with respect to nearby first-order approximations of invariant tori. This tracking error definition enables the straightforward design of reference trajectories for formation flying on quasi-periodic orbits and gain selection based on geometric insight. Numerical simulations apply the controller to stabilize a spacecraft on a torus relative to a periodic orbit for low control effort.

INTRODUCTION

As spacecraft increasingly operate within complex multi-body environments, efficient control of formations of spacecraft will be a key capability for missions such as space station assembly, stereographic heliophysics observations, distributed astronomy telescopes, or distributed antenna systems. While orbits in predominantly two-body environments are well approximated by conics, multi-body environments admit a more complex solution space. The Circular Restricted Three-Body Problem (CR3BP) supplies a useful approximation for preliminary analysis of the motion of spacecraft in a three-body environment, such as the Earth-Moon or Sun-Earth system, formulated in a rotating frame defined by the two primary bodies. Within the CR3BP, periodic orbits exhibit periodicity in the rotating frame, and have been leveraged in the trajectory design of currently operating spacecraft including the Deep Space Climate Observatory[1] and Gaia,[2] as well as future missions such as the Nancy Grace Roman Space Telescope[3] and James Webb Space Telescope.[4] Compared to orbits in two-body environments, where heuristics on spacecraft relative motion are well known, spacecraft motion relative to a periodic orbit in a multi-body system is more challenging to characterize due to the complex and chaotic nature of the solution space. Stabilizing control schemes that incorporate insight into multi-body dynamics will be essential for station-keeping, rendezvous, and proximity operations for spacecraft relative to a periodic orbit.

Strategies for the design and control of spacecraft formations in the CR3BP have historically leveraged the quasi-periodic orbits that exist near periodic orbits with oscillatory modes. This strategy was introduced by Barden and Howell and demonstrated that spacecraft on quasi-periodic orbits in the CR3BP remain naturally bounded near a periodic orbit as the spacecraft wind along the associated torus.[5] However, as demonstrated by Kolemen et al.[6] and Olikara and Scheeres,[7] the compu-

*Graduate Research Assistant, Colorado Center for Astrodynamics Research, Smead Aerospace Engineering Sciences, University of Colorado Boulder, Boulder, CO 80303

†Assistant Professor, Colorado Center for Astrodynamics Research, Smead Aerospace Engineering Sciences, University of Colorado Boulder, Boulder, CO 80303

tation of quasi-periodic orbits in the CR3BP is an expensive numerical process. A study by Baresi et al. found that using first-order approximations of quasi-periodic motion relative to periodic orbits provides near-bounded relative motion in nonlinear dynamical systems;[8] these approximations also serve as a computationally inexpensive alternative for small separations from a periodic orbit. Using these results as a foundation, Elliott and Bosanac introduced a coordinate transformation for the motion of a spacecraft in the CR3BP formulated using first-order quasi-periodic motion near a periodic orbit.[9] This coordinate set provides a computationally inexpensive and straightforward definition of a state along a first-order approximation of an invariant torus, and provides a time-invariant state description for a trajectory tracing along the torus for dynamics linearized about the periodic orbit. However, in the nonlinear CR3BP, small deviations from quasi-periodic orbits that exist near periodic orbits that also possess unstable modes may result in diverging and chaotic trajectories.

Due to the sensitivity of multi-body environments, control is often essential to maintain a desired spacecraft formation. Previous investigations into the control of spacecraft formations in three-body environments have been conducted by several authors. Optimal control techniques have been applied to stabilize a formation of spacecraft near unstable orbits in the CR3BP by Marchand and Howell,[10] Millard and Howell,[11] and Bando and Ichikawa,[12] demonstrating that low control effort is required to maintain spacecraft formations in sensitive environments. Scheeres et al. developed a control law to stabilize the motion of a spacecraft around an unstable periodic orbit in the Hill three-body problem by incorporating stability information via the eigenvectors of the monodromy matrix of the periodic orbit corresponding to the stable and unstable modes.[13] This nontraditional control formulation motivates further exploration of the use of information from the monodromy matrix of a periodic orbit within control design in multi-body environments.

Within two-body environments, incorporation of geometric state representations has been demonstrated to supply additional insight into control law design. Previous studies have been conducted on the use of relative orbital element sets for formation flying control in predominately two-body environments by Breger and How,[14] Gaias and D'Amico,[15] and Bennett and Schaub.[16] One method for deriving stabilizing feedback control leverages control Lyapunov functions, which can produce asymptotically converging tracking control.[17] While control Lyapunov functions for spacecraft control are often formulated via Cartesian states,[18,19] control Lyapunov functions may be developed in terms of other state representations, such as Keplerian orbital elements.[20] The results of control laws developed via Lyapunov functions for two-body environments motivate further application of control Lyapunov functions in three-body environments with alternative state representations.

In this paper, the geometric relative coordinate set introduced by Elliott and Bosanac[9] is used to develop a feedback control law in the CR3BP for formation flying relative to a periodic orbit that admits nearby quasi-periodic orbits. The geometric coordinates and respective coordinate rates describe the state of a spacecraft relative to a periodic orbit in the CR3BP with respect to first-order quasi-periodic motion in a local Hill frame. Low computational effort is required to compute the geometric coordinates compared to the computation of nonlinear quasi-periodic motion. Thus, the geometric coordinate set enables the rapid and intuitive definition of reference trajectories. These reference trajectories support various relative motion objectives, including station-keeping along a quasi-periodic orbit, maneuvering between quasi-periodic orbits of different size relative to the periodic orbit, and controlling rotation rates along a torus. This geometric relative coordinate set is used to derive a feedback control law that defines feedback error in terms of the coordinates and coordinate rates to leverages the geometric insight of the relative coordinates. Numerical simulations of the control law are presented to demonstrate asymptotic convergence to a reference trajectory in the CR3BP and to analyze an example of the effects of perturbing accelerations unknown to the control system. Finally, the geometric coordinate based control law is compared to a Cartesian state control law to compare and contrast the responses of the two controller when stabilizing to the same reference trajectory.

SPACECRAFT FORMATION DYNAMICS

In this analysis, the natural dynamics of a spacecraft are assumed to be governed by the CR3BP with perturbing accelerations. Two spacecraft are defined: a target spacecraft, denoted by subscript t, and a chaser spacecraft, denoted by subscript c. The motion of the target spacecraft is described using the equations of motion of the CR3BP formulated in the rotating frame. The target spacecraft is assumed to be uncontrolled, following a reference periodic orbit with an oscillatory mode. The motion of the chaser spacecraft in the CR3BP is described relative to the target spacecraft using equations of relative motion formulated in a Hill frame defined using the target spacecraft. The stability of the reference periodic orbit is used to map the relative position and velocity of the chaser spacecraft to relative coordinates and coordinate rates for use within the feedback control law.

The Circular Restricted Three-Body Problem

The CR3BP supplies an autonomous description of the uncontrolled dynamics of a single spacecraft in the presence of two celestial bodies. The bodies, labeled primaries, are modeled as point masses following circular orbits about their mutual barycenter. The more massive primary is labeled P_1 while the less massive primary is labeled P_2. A nondimensionalization scheme is commonly employed for quantities of length, time, and mass in the CR3BP: quantities of length are normalized such that the distance between the primary bodies is unity, quantities of time are normalized such that the mean motion of the system is equal to unity, and quantities of mass are normalized by the total mass of the primary system. As a result of the nondimensionalization scheme, a system mass ratio, μ is defined as $\mu = m_2/(m_1 + m_2)$, where m_1 is the mass of P_1 and m_2 is the mass of P_2. A rotating coordinate frame, denoted as $R : \{\hat{\boldsymbol{x}}, \hat{\boldsymbol{y}}, \hat{\boldsymbol{z}}\}$, is also defined to rotate with the two primary bodies with respect to an inertial frame, denoted as $N : \{\hat{\boldsymbol{X}}, \hat{\boldsymbol{Y}}, \hat{\boldsymbol{Z}}\}$. The first axis of the rotating frame, $\hat{\boldsymbol{x}}$, is directed to P_2 from P_1. The third axis of the rotating frame, $\hat{\boldsymbol{z}}$ is defined in the direction of the total orbital angular momentum of the primary system and such that $\hat{\boldsymbol{z}} = \hat{\boldsymbol{Z}}$. Finally, the second axis of the rotating frame, $\hat{\boldsymbol{y}}$, completes the right-handed orthogonal coordinate frame. A spacecraft, P_3, is modeled as a point mass of negligible mass, described by a state vector, $\boldsymbol{x} = [x, y, z, \dot{x}, \dot{y}, \dot{z}]^T$, defined relative to the system barycenter. The position vector of each body relative to the system barycenter is denoted as $\boldsymbol{r}_i$. The equations of motion for a spacecraft in the CR3BP are formulated in the rotating frame and expressed as[21]

$$\ddot{x} = 2\dot{y} + \frac{\partial U^*}{\partial x}, \qquad \ddot{y} = -2\dot{x} + \frac{\partial U^*}{\partial y}, \qquad \ddot{z} = \frac{\partial U^*}{\partial z} \tag{1}$$

where U^* is a pseudo-potential function, defined as

$$U^* = \frac{1}{2}\left(x^2 + y^2\right) + \frac{1-\mu}{r_{13}} + \frac{\mu}{r_{23}} \tag{2}$$

The quantities r_{13} and r_{23} are the distances of the spacecraft from P_1 and P_2 respectively, defined as $r_{13} = |\boldsymbol{r}_3 - \boldsymbol{r}_1|$ and $r_{23} = |\boldsymbol{r}_3 - \boldsymbol{r}_2|$. This autonomous description of the motion of a spacecraft renders the CR3BP valuable for preliminary spacecraft trajectory design in a three-body system due to the existence of fundamental dynamical structures such as equilibrium points, periodic orbits, and quasi-periodic orbits.

Equations of Relative Motion in the CR3BP

Equations of relative motion enable the direct integration of the motion of the chaser spacecraft relative to the target spacecraft. The CR3BP is reformulated in a Hill frame that is defined using the inertial state of the target spacecraft relative to P_2. The Hill frame is denoted as $O : \{\hat{\boldsymbol{o}}_r, \hat{\boldsymbol{o}}_\theta, \hat{\boldsymbol{o}}_h\}$ where $\hat{\boldsymbol{o}}_r$ is the "radial" direction, $\hat{\boldsymbol{o}}_\theta$ is the "along-track" direction, and $\hat{\boldsymbol{o}}_h$ is the "cross-track" direction. These three basis vectors are defined as

$$\hat{\boldsymbol{o}}_r = \frac{\boldsymbol{r}_{2t}}{r_{2t}}, \qquad \hat{\boldsymbol{o}}_\theta = \hat{\boldsymbol{o}}_h \times \hat{\boldsymbol{o}}_r, \qquad \hat{\boldsymbol{o}}_h = \frac{\boldsymbol{h}_{2t}}{h_{2t}} \tag{3}$$

where $\boldsymbol{r}_{2t}$ is the position of the target spacecraft relative to P_2. In addition, $\boldsymbol{h}_{2t}$ is the inertial orbital angular momentum of the spacecraft relative to P_2, defined as $\boldsymbol{h}_{2t} = \boldsymbol{r}_{2t} \times \dot{\boldsymbol{r}}_{2t}$, where $\dot{\boldsymbol{r}}_{2t}$ is the inertial velocity of the target spacecraft relative to P_2. The position of the chaser spacecraft relative to the target spacecraft, $\boldsymbol{\rho}$, is defined as $\boldsymbol{\rho} = \boldsymbol{r}_c - \boldsymbol{r}_t$, where $\boldsymbol{r}_t$ and $\boldsymbol{r}_c$ are the position vectors of the target and chaser spacecraft, respectively. The natural relative acceleration, $\boldsymbol{f}$, between the chaser and target spacecraft in the CR3BP for an observer fixed in the Hill frame is expressed as[9]

$$\boldsymbol{f} = \ddot{\boldsymbol{\rho}} - \dot{\boldsymbol{\omega}}_{ON} \times \boldsymbol{\rho} - 2\big(\boldsymbol{\omega}_{ON} \times \boldsymbol{\rho}'\big) - \boldsymbol{\omega}_{ON} \times \big(\boldsymbol{\omega}_{ON} \times \boldsymbol{\rho}\big) \tag{4}$$

where $\boldsymbol{\rho}'$ is the relative velocity for an observer fixed in the Hill frame. The natural relative acceleration, $\ddot{\boldsymbol{\rho}}$, between the chaser and target spacecraft in the CR3BP for an observer in the inertial frame is defined in terms of nondimensional quantities as

$$\ddot{\boldsymbol{\rho}} = -\mu \left(\frac{\boldsymbol{r}_{2c}}{r_{2c}^3} - \frac{\boldsymbol{r}_{2t}}{r_{2t}^3} \right) - (1-\mu) \left(\frac{\boldsymbol{r}_{1c}}{r_{1c}^3} - \frac{\boldsymbol{r}_{1t}}{r_{1t}^3} \right) \tag{5}$$

where the shorthand notation ${}^N d^2/dt^2(\boldsymbol{\rho}) = \ddot{\boldsymbol{\rho}}$ is used to denote vector differentiation with respect to the inertial frame. The angular velocity of the Hill frame with respect to the inertial frame is denoted $\boldsymbol{\omega}_{ON}$ and the respective time rate of change is denoted $\dot{\boldsymbol{\omega}}_{ON}$; expressions for these vector quantities are presented by Elliott and Bosanac.[9] The total relative acceleration of the chaser spacecraft for an observer fixed in the Hill frame, $\boldsymbol{\rho}''$, is influenced by the gravitational influence of P_1 and P_2 captured in $\boldsymbol{f}$, the control acceleration, $\boldsymbol{u}$, and perturbing accelerations, $\boldsymbol{d}$. Using these definitions, the total relative acceleration is written as

$$\boldsymbol{\rho}'' = \boldsymbol{f} + \boldsymbol{u} + \boldsymbol{d} \tag{6}$$

Note that $\boldsymbol{d}$ includes all accelerations not modeled within the derivation of the controller. In this formulation of the dynamical environment, a 6×1 Cartesian state vector, $\boldsymbol{q}$, that describes the state of the chaser spacecraft relative to the target spacecraft expressed in the Hill frame is defined as

$$\boldsymbol{q} = \begin{bmatrix} \boldsymbol{\rho} \\ \boldsymbol{\rho}' \end{bmatrix} \tag{7}$$

Since the equations of relative motion are a function of the instantaneous state of the target spacecraft, the relative state between the chaser and target spacecraft is integrated simultaneously with the state of the target spacecraft. The target spacecraft state formulated in the rotating frame, $\boldsymbol{x}_c$, and the state of the chaser spacecraft relative to the target spacecraft formulated in the Hill frame, $\boldsymbol{q}$, are combined within an augmented state vector, $\boldsymbol{y}$, defined as

$$\boldsymbol{y} = \begin{bmatrix} \boldsymbol{x}_c \\ \boldsymbol{q} \end{bmatrix} \tag{8}$$

When the state of the target spacecraft is integrated via the equations of motion of the CR3BP from Eq. (1) and the relative chaser spacecraft is integrated via the formulated equations of relative motion from Eq. (6), the rate of change of $\boldsymbol{y}$ is expressed as a system of 12 scalar, autonomous differential equations for numerical integration.

Summary of Geometric Relative Coordinates

The geometric relative coordinate set introduced by Elliott and Bosanac leverage a description of quasi-periodic motion emanating from a periodic orbit in the CR3BP through the complex eigenvector of the monodromy matrix of the periodic orbit. The eigenvector corresponding to the complex eigenspace of the monodromy matrix of the periodic orbit expressed in the Hill frame, $\tilde{\boldsymbol{q}}$, is written in terms of real and imaginary components as $\tilde{\boldsymbol{q}} = \tilde{\boldsymbol{q}}_r \pm i\,\tilde{\boldsymbol{q}}_i$. The real and imaginary components of the complex eigenvector are expressed as

$$\tilde{\boldsymbol{q}}_r = \begin{bmatrix} \boldsymbol{r}_r \\ \boldsymbol{v}_r \end{bmatrix}, \qquad \tilde{\boldsymbol{q}}_i = \begin{bmatrix} \boldsymbol{r}_i \\ \boldsymbol{v}_i \end{bmatrix} \tag{9}$$

where $\boldsymbol{r}$ and $\boldsymbol{v}$ indicate position and velocity components of the eigenvector, respectively, and subscripts r and i indicate real and imaginary components respectively. The time rate of change of the complex eigenvector for an observer fixed in the Hill frame, $\tilde{\boldsymbol{q}}'$, is computed using the Jacobian, $[A] = \partial\boldsymbol{q}'/\partial\boldsymbol{q}$, evaluated at the periodic orbit as $\tilde{\boldsymbol{q}}' = [A]\tilde{\boldsymbol{q}}$. This rate of change is also written in terms of real and imaginary components as $\tilde{\boldsymbol{q}}' = \tilde{\boldsymbol{q}}_r' \pm i\,\tilde{\boldsymbol{q}}_i'$. The real and imaginary rate of changes of the eigenvector are expressed as vectors corresponding to the velocity, $\boldsymbol{v}$, and acceleration, $\boldsymbol{a}$, components as

$$\tilde{\boldsymbol{q}}_r' = \begin{bmatrix} \boldsymbol{v}_r \\ \boldsymbol{a}_r \end{bmatrix}, \qquad \tilde{\boldsymbol{q}}_i' = \begin{bmatrix} \boldsymbol{v}_i \\ \boldsymbol{a}_i \end{bmatrix} \tag{10}$$

Exciting the oscillatory mode expressed in the Hill frame produces motion relative to the periodic orbit that lies within the center eigenspace. In configuration space, a unit vector perpendicular to the plane that spans the center eigenspace is defined as

$$\hat{\boldsymbol{n}} = \frac{\boldsymbol{r}_r \times \boldsymbol{r}_i}{|\boldsymbol{r}_r \times \boldsymbol{r}_i|} \tag{11}$$

The first and second time derivatives of the normal vector for an observer in the Hill frame, $\hat{\boldsymbol{n}}'$ and $\hat{\boldsymbol{n}}''$ respectively, are calculated by differentiating this expression for $\hat{\boldsymbol{n}}$ with respect to time.

The complex eigenvector contains information about the oscillatory mode of the periodic orbit and is employed to map between Cartesian states and the geometric relative coordinates set. In this paper, the monodromy matrix of the reference periodic orbit is assumed to possess at least one pair of complex conjugate eigenvalues that lie on the unit circle, corresponding to an oscillatory mode. If more that one pair of complex conjugate eigenvalues exist, indicating the presence of two oscillatory modes, one of the two modes must be selected for use with the coordinate set. However, for some periodic orbits in the CR3BP, the orbit may possess an oscillatory mode that only span the $\hat{\boldsymbol{o}}_h$ direction in configuration space. Motion along this mode is rectilinear as seen by the Hill frame, and not considered within the scope of this paper. Incorporating information on the oscillatory mode for use with the presented control law is implemented by simultaneously integrating the corresponding complex eigenvector via the Jacobian with the states of the target and chaser spacecraft to form a system of 18 scalar and autonomous differential equations.

The geometric relative coordinate set introduced by Elliott and Bosanac consists of three quantities that describe the position of the chaser spacecraft with respect to the target spacecraft relative to first-order quasi-periodic motion. The first coordinate, h, is the distance of the chaser spacecraft from the plane that spans the center eigenspace in configuration space, measured along the $\hat{\boldsymbol{n}}$ axis. The second and third coordinates, ε and θ respectively, correspond to the amplitude and phase shift of the oscillatory motion that intersects the position of the chaser spacecraft projected onto the center eigenspace. The geometric coordinates are summarized in a 3×1 set of coordinates, $\boldsymbol{e}$, and a 3×1 set of coordinate rates, $\dot{\boldsymbol{e}}$, defined as

$$\boldsymbol{e} = \begin{bmatrix} h \\ \varepsilon \\ \theta \end{bmatrix}, \qquad \dot{\boldsymbol{e}} = \begin{bmatrix} \dot{h} \\ \dot{\varepsilon} \\ \dot{\theta} \end{bmatrix} \tag{12}$$

The three coordinates and their respective time rates of change form a six-dimensional state description of motion relative to a periodic orbit with an oscillatory mode. A conceptual illustration of the relative position appears in Figure 1(a) using a Cartesian description and Figure 1(b) using the geometric relative coordinates. Compared to a Cartesian state description, the geometric relative coordinates supply an additional layer of intuition into relative motion near periodic orbits in the context of the center eigenspace.

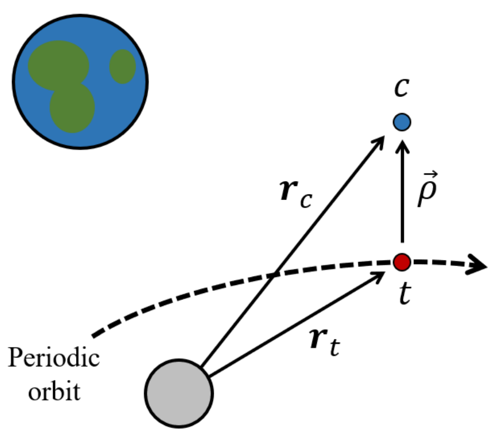

(a) Relative Cartesian states.

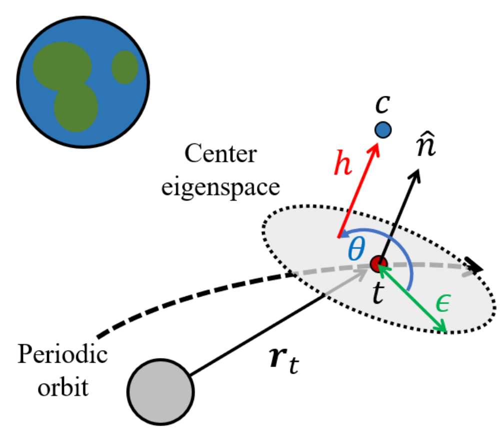

(b) Geometric relative coordinates.

Figure 1. Comparison of relative Cartesian state description and relative coordinate description around a periodic orbit with oscillatory modes.

The description of a first-order quasi-periodic orbit relative to the periodic orbit is straightforward via the geometric coordinate set. In fact, for dynamics linearized about the periodic orbit, a trajectory tracing the surface of a torus is represented by a time-invariant state description. This time-invariant set corresponds to $h = \dot{h} = \dot{\varepsilon} = \dot{\theta} = 0$. The remaining two coordinates, ε and θ, are free parameters corresponding to the size of the torus and angle from an invariant curve along the torus respectively. As an example of the reference motion defined by the linear invariant set, the geometric relative coordinates are used to approximate quasi-periodic motion relative to a southern L_2 halo orbit in the Earth-Moon CR3BP. This reference orbit is visualized using dimensional quantities in Figure 2(a) relative to the Moon and expressed in the Earth-Moon rotating frame. This halo orbit possesses a nontrivial pair of eigenvalues of the monodromy matrix that indicate an oscillatory mode, and therefore the presence of nearby quasi-periodic orbits. Three first-order approximations of quasi-periodic orbits are depicted in the Hill frame in Figure 2(b) relative to the periodic orbit, represented as a black marker. The associated tori correspond to constant values of ε: $\varepsilon = 1$ km (red), $\varepsilon = 5$ km (magenta), and $\varepsilon = 10$ km (blue). While the surface of these tori form complex dynamical structures in the six-dimensional phase space, a trajectory tracing the surface of a torus is straightforwardly defined via the geometric coordinates. In the nonlinear CR3BP, natural motion initialized on these tori will gradually diverge from these references. However, when the separation between the two spacecraft is small, the coordinate set provides an intuitive and straightforward definition of quasi-periodic orbits for use in the presented feedback control law.

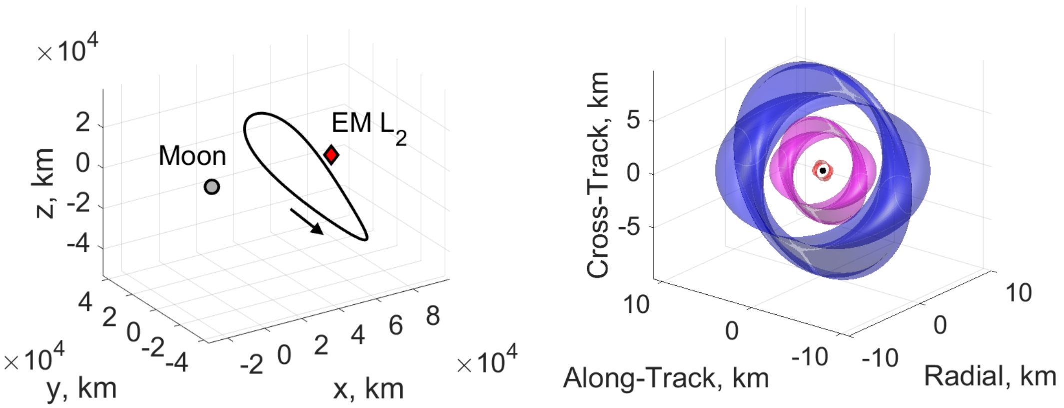

(a) An Earth-Moon L_2 halo orbit.

(b) First-order invariant tori relative to the halo orbit.

Figure 2. First-order approximation of invariant tori relative to an Earth-Moon halo orbit defined using constant values of ε.

Geometric Relative Coordinate Dynamics

The geometric relative coordinates and coordinate rates map from Cartesian position and velocity state components relative to the target spacecraft expressed in the Hill frame and vice versa. The mapping from geometric coordinates to a relative position vector expressed in Cartesian coordinates is written as[9]

$$\boldsymbol{\rho} = h\hat{\boldsymbol{n}} + \varepsilon\left(\boldsymbol{r}_r \cos\theta + \boldsymbol{r}_i \sin\theta\right) \tag{13}$$

Differentiating Eq. (13), the associated relative velocity for an observer in the Hill frame, $\boldsymbol{\rho}'$, is written in terms of geometric relative coordinates and coordinate rates as[9]

$$\boldsymbol{\rho}' = h\hat{\boldsymbol{n}}' + \dot{h}\hat{\boldsymbol{n}} + \dot{\varepsilon}\left(\boldsymbol{r}_r \cos\theta + \boldsymbol{r}_i \sin\theta\right) + \varepsilon\left(\boldsymbol{v}_r \cos\theta - \boldsymbol{r}_r\dot{\theta}\sin\theta + \boldsymbol{v}_i \sin\theta + \boldsymbol{r}_i\dot{\theta}\cos\theta\right) \tag{14}$$

A nonunique mapping occurs when the spacecraft lies along the $\hat{\boldsymbol{n}}$ axis. In this case, $\varepsilon = 0$ and θ is undefined, producing a singularity in the inverse mapping from relative position and velocity to geometric coordinates and rates.[9] To avoid this singularity, a nonsingular coordinate set, $\boldsymbol{z}$, and nonsingular coordinate rate set, $\dot{\boldsymbol{z}}$, is also introduced by Elliott and Bosanac and defined as[9]

$$\boldsymbol{z} = \begin{bmatrix} h \\ \alpha \\ \beta \end{bmatrix}, \qquad \dot{\boldsymbol{z}} = \begin{bmatrix} \dot{h} \\ \dot{\alpha} \\ \dot{\beta} \end{bmatrix} \tag{15}$$

where $\alpha = \varepsilon \cos\theta$ and $\beta = \varepsilon \sin\theta$. The relative position vector can be expressed as a linear combination of the nonsingular coordinates and components of the complex eigenvector as

$$\boldsymbol{\rho} = [R]\boldsymbol{z} \tag{16}$$

where $[R]$ is a 3×3 matrix that spans the configuration space, written as

$$[R] = \begin{bmatrix} \hat{\boldsymbol{n}} & \boldsymbol{r}_r & \boldsymbol{r}_i \end{bmatrix} \tag{17}$$

The first and second time derivatives of this matrix, $[\dot{R}]$ and $[\ddot{R}]$, respectively, are computed as

$$[\dot{R}] = \begin{bmatrix} \hat{\boldsymbol{n}}' & \boldsymbol{v}_r & \boldsymbol{v}_i \end{bmatrix}, \tag{18}$$

$$[\ddot{R}] = \begin{bmatrix} \hat{\boldsymbol{n}}'' & \boldsymbol{a}_r & \boldsymbol{a}_i \end{bmatrix} \tag{19}$$

The nonsingular coordinate set, the $[R]$ matrix, and respective time derivatives, are used within the control law derivation to transform between geometric coordinates and Cartesian states.

To compute the acceleration of the geometric coordinates due to the gravitational effects of the two primary bodies, recall the expression for relative velocity in terms of geometric coordinates and coordinate rates, as defined in Eq. (14). This expression is equivalently written as

$$\boldsymbol{\rho}' = [\dot{R}]\boldsymbol{z} + [B]\dot{\boldsymbol{e}} \tag{20}$$

where $[B]$ is a 3×3 matrix, denoted the control influence matrix, defined as

$$[B] = \begin{bmatrix} \hat{\boldsymbol{n}} & (\boldsymbol{r}_r \cos\theta + \boldsymbol{r}_i \sin\theta) & \varepsilon\left(\boldsymbol{r}_i \cos\theta - \boldsymbol{r}_r \sin\theta\right) \end{bmatrix} \tag{21}$$

Equating the time derivative of the right hand side of Eq. (20) to the sum of the relative acceleration, $\boldsymbol{f}$, due to the CR3BP formulated in the Hill frame and a control acceleration, $\boldsymbol{u}$, the resulting condition holds:

$$\boldsymbol{f} + \boldsymbol{u} = [\ddot{R}]\boldsymbol{z} + [\dot{R}]\dot{\boldsymbol{z}} + [\dot{B}]\dot{\boldsymbol{e}} + [B]\ddot{\boldsymbol{e}} \tag{22}$$

where the right hand side consists of the four terms of the product rule derivative of the two terms in Eq. (20). The time derivative of $[B]$ is found by directly differentiating the columns of the matrix. The acceleration, $\ddot{\boldsymbol{e}}$, is defined as the acceleration of the geometric coordinates due to both the gravitational influences of P_1 and P_2 and a control acceleration. Solving for $\ddot{\boldsymbol{e}}$ in Eq. (22), the acceleration is written as

$$\ddot{\boldsymbol{e}} = \ddot{\boldsymbol{e}}^* + [B]^{-1}\boldsymbol{u} \tag{23}$$

where the acceleration, $\ddot{\boldsymbol{e}}^*$, is the natural acceleration of the geometric coordinates, defined as

$$\ddot{\boldsymbol{e}}^* = [B]^{-1}\left(\boldsymbol{f} - [\ddot{R}]\boldsymbol{z} - [\dot{R}]\dot{\boldsymbol{z}} - [\dot{B}]\dot{\boldsymbol{e}}\right) \tag{24}$$

With the total acceleration of the geometric coordinates defined in terms of a Cartesian control acceleration vector, the feedback control law is derived via a control Lyapunov function.

FEEDBACK CONTROL LAW DERIVATION

In this section, a control law is analytically derived via a control Lyapunov function formulated using geometric relative coordinates and coordinate rates. The controller is designed to track a specified desired trajectory relative to a periodic orbit that admits an oscillatory mode in the CR3BP. A quadratic Lyapunov function is selected to produce globally asymptotically convergence to the desired trajectory without any constraints on control effort.[17] This Lyapunov function produces a control law with similar structure to Cartesian state feedback control laws.[18,20]

Control Lyapunov Function

A Lyapunov function is selected as a function of relative geometric coordinate and coordinate rate tracking errors. The coordinate tracking error, $\delta\boldsymbol{e}$, and the coordinate rate tracking error, $\delta\dot{\boldsymbol{e}}$, are defined as

$$\delta\boldsymbol{e} = \boldsymbol{e} - \boldsymbol{e}_d, \qquad \delta\dot{\boldsymbol{e}} = \dot{\boldsymbol{e}} - \dot{\boldsymbol{e}}_d \tag{25}$$

where $\boldsymbol{e}_d$ and $\dot{\boldsymbol{e}}_d$ are the desired coordinates and coordinate rates respectively. Following a similar procedure for previously derived Cartesian control laws,[19] the Lyapunov function, V, is defined as a radially unbounded, positive definite function of geometric coordinate and coordinate rate tracking errors as

$$V(\delta\boldsymbol{e}, \delta\dot{\boldsymbol{e}}) = \frac{1}{2}\delta\boldsymbol{e}^T[K_1]\delta\boldsymbol{e} + \frac{1}{2}\delta\dot{\boldsymbol{e}}^T\delta\dot{\boldsymbol{e}} \tag{26}$$

where $[K_1]$ is a positive definite 3×3 gain matrix applied to the coordinates. The time derivative of V is

$$\dot{V} = \delta\dot{\boldsymbol{e}}^T\left([K_1]\delta\boldsymbol{e} + \delta\ddot{\boldsymbol{e}}\right) \tag{27}$$

where the acceleration error term, $\delta\ddot{\boldsymbol{e}}$, is the difference between the controlled acceleration of the chaser spacecraft, and the desired acceleration, $\ddot{\boldsymbol{e}}_d$, written as

$$\delta\ddot{\boldsymbol{e}} = \ddot{\boldsymbol{e}} - \ddot{\boldsymbol{e}}_d = \ddot{\boldsymbol{e}}^* + [B]^{-1}\boldsymbol{u} - \ddot{\boldsymbol{e}}_d \tag{28}$$

Continuing an analogous procedure to Cartesian control law derivations, the presented control law is selected to force the the first time derivative of the Lyapunov function equal to a negative definite function of the coordinate rates,[19] defined as

$$\dot{V}(\delta\dot{\boldsymbol{e}}) = -\delta\dot{\boldsymbol{e}}^T[K_2]\delta\dot{\boldsymbol{e}} \tag{29}$$

where $[K_2]$ is a positive definite 3×3 coordinate rate feedback gain matrix. Equating Eq. (27) and Eq. (29) and solving for $\boldsymbol{u}$, the resulting tracking control law is

$$\boldsymbol{u} = -[B]\Big([K_1]\delta\boldsymbol{e} + [K_2]\delta\dot{\boldsymbol{e}} + \ddot{\boldsymbol{e}}^* - \ddot{\boldsymbol{e}}_d\Big) \tag{30}$$

For a trajectory tracing a first-order approximation of an invariant torus, the acceleration of the geometric coordinates for dynamics linearized about the periodic orbit is equal to zero. When tracking this motion, the desired chaser acceleration is $\ddot{\boldsymbol{e}}_d = \boldsymbol{0}$ and the control law simplifies to

$$\boldsymbol{u} = -[B]\Big([K_1]\delta\boldsymbol{e} + [K_2]\delta\dot{\boldsymbol{e}} + \ddot{\boldsymbol{e}}^*\Big) \tag{31}$$

In this form, the control law resembles the structure of a proportional-derivative controller and feed-forward acceleration term, with a mapping from error defined in terms of coordinates and coordinate rates to a Cartesian acceleration vector via the control influence matrix. The asymptotic stability of the control law is verified by confirming that the first nonzero derivative of V evaluated on the set $\delta\dot{\boldsymbol{e}} = \boldsymbol{0}$ is a negative definition function of $\delta\boldsymbol{e}$.[19] The third derivative of V is found as

$$\dddot{V}(\delta\dot{\boldsymbol{e}} = \boldsymbol{0}) = -2\delta\boldsymbol{e}^T[K_1]^T[K_2][K_1]\delta\boldsymbol{e} \tag{32}$$

which is a negative definite function of $\delta\boldsymbol{e}$, verifying that the control law is asymptotically stabilizing to the desired state for a spacecraft formation in the CR3BP. Furthermore, despite the non-unique mapping that exists when $\varepsilon = 0$, the geometric coordinate control law is able to asymptotically approach $\varepsilon = 0$. As ε approaches zero, θ and angle error approach undefined values. However, as ε approaches zero, the magnitude of the column of the control influence matrix from Eq. (21) which determines effort spent on correcting the angle error also approaches zero. Thus, the control law is observed to allow asymptotic regulation to the periodic orbit.

The geometric interpretation of tracking error and control gains enables a wide range of reference trajectories and control responses to be intuitively designed to achieve different formation flying objectives. In this formulation, gain matrices $[K_1]$ and $[K_2]$ may be manually tuned to achieve the desired control response with respect to quasi-periodic motion relative to a periodic orbit. The control law uses no additional linearization assumptions beyond the linear approximations within the definition of the geometric coordinates. However, tracking first-order quasi-periodic motion relative to a periodic orbit, as opposed to a path in the nonlinear system, results in small steady-state control usage. In addition, unknown perturbing accelerations on the chaser spacecraft will result in steady-state tracking error and control usage. In the following section, examples of the controller's performance in the CR3BP with and without perturbations are explored via numerical simulations.

NUMERICAL SIMULATIONS

Three numerical examples are explored to demonstrate the performance of the control law formulated using geometric relative coordinate. The first example focuses on analyzing the performance of the controller to demonstrate asymptotic convergence of the chaser spacecraft to a reference trajectory defined relative to a target spacecraft following a halo orbit in the Earth-Moon CR3BP. The second example is formulated to study the performance of the control law in the Sun-Earth CR3BP with solar radiation pressure (SRP) as an unknown perturbing acceleration. In this example, two chaser spacecraft operate on quasi-periodic orbits relative to an empty formation center that is located along a Sun-Earth halo orbit in the natural CR3BP. Finally, the third example compares the performance of the geometric coordinate control law to a Cartesian state control law for the same desired formation reconfiguration maneuver in the unperturbed Earth-Moon CR3BP.

Station-Keeping near an Earth-Moon L_2 Halo Orbit

A spacecraft formation near an unstable Earth-Moon southern L_2 halo orbit is used to demonstrate the asymptotic stability of the designed control law in tracking a reference trajectory defined using geometric coordinates in the CR3BP. The target spacecraft follows an Earth-Moon L_2 halo orbit, illustrated relative to the Moon in the rotating frame in Figure 2. This orbit possesses a period in the rotating frame of approximately $T = 14.5$ days. A stability analysis of this halo orbit reveals an unstable mode such that the relative motion environment about the periodic orbit is unstable and an oscillatory mode, indicating the existence of nearby quasi-periodic orbits. This oscillatory mode enables the use of the geometric coordinate set and the designed control law.

The goal of the chaser spacecraft is to maneuver to a desired trajectory along a first-order approximation of an invariant torus given a small initial error. The initial state of the target spacecraft is defined at the apolune of the halo orbit. Concurrently, the chaser spacecraft is slightly perturbed from this state to demonstrate the capability of the controller to ensure asymptotic convergence towards the desired trajectory. The initial conditions of the chaser spacecraft relative to the target spacecraft are defined using geometric coordinates and listed in Table 1 along with the desired values. Without control, the natural motion of the chaser spacecraft from the initial conditions departs the vicinity of the target spacecraft. The control gains are manually tuned to achieve the desired controlled response of the chaser spacecraft. For this example, the nondimensional coordinate gains are selected as $[K_1] = 1000\ [I_3]$ and the coordinate rate gains are selected as $[K_2] = 500\ [I_3]$, where $[I_3]$ is the 3×3 identity matrix.

Table 1. Initial and desired values of the geometric coordinates for the chaser spacecraft relative to a target spacecraft following an Earth-Moon L_2 halo orbit.

Quantity	Initial Value	Desired Value
h	-2 km	0 km
ε	10.1 km	10 km
θ	0.02 rad	0 rad
$\dot{h}$	0.003 km/s	0 km/s
$\dot{\varepsilon}$	-0.001 km/s	0 km/s
$\dot{\theta}$	0 rad/s	0 rad/s

With initial conditions for the target and chaser spacecraft defined, the controlled response of the formation is analyzed. The natural motion of the target spacecraft and controlled motion of the chaser spacecraft are propagated for one period of the halo orbit. The trajectory of the chaser spacecraft controlled using the control law expressed in Eq. (31) is displayed in Figure 3 relative to the target spacecraft in the Hill frame. The target spacecraft is represented by a black marker and the trajectory of the chaser spacecraft is plotted in blue. In this example, the control law demonstrates asymptotic convergence to the desired reference trajectory, resulting in relative motion that remains near the target spacecraft. The relative state of the chaser spacecraft over time, expressed in geometric relative coordinates, is plotted in Figure 4 in blue with the desired reference trajectory represented in black.

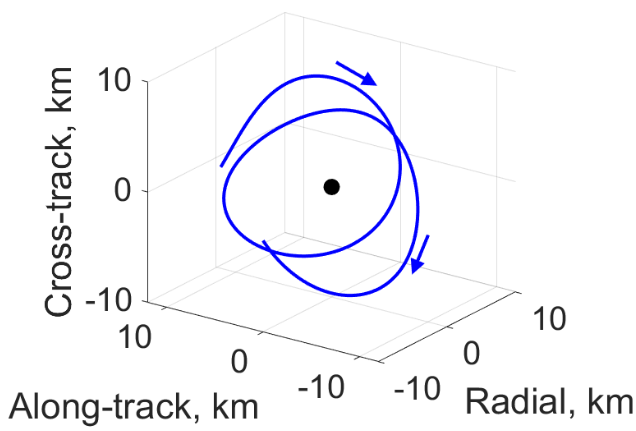

Figure 3. Controlled trajectory of the chaser spacecraft relative to the target spacecraft on the Earth-Moon halo orbit.

While the controlled trajectory of the chaser spacecraft is observed to approach the desired trajectory, analysis of the error terms of the control Lyapunov function confirm asymptotic convergence. The error terms of the Lyapunov function, $\delta \boldsymbol{e}$ (blue) and $\delta \dot{\boldsymbol{e}}$ (red), are plotted over time in Figure 5(a) on a logarithmic scale to visualize asymptotic convergence to within expected numerical tolerances. The magnitude of the control acceleration over time is also plotted in Figure 5(b) on a logarithmic scale. As expected, due to the linear approximations inherent to the definition of the geometric coordinates, a steady-state control usage is observed. However, for this example, the order of magnitude of the steady-state acceleration is 10^{-10} m/s^2. This small required control acceleration results from the differences between the desired trajectory defining a first-order quasi-periodic orbit, and a quasi-periodic orbit in the nonlinear CR3BP. In future work, incorporation of a control deadband can be modeled to analyze the implementation of the small required control acceleration.

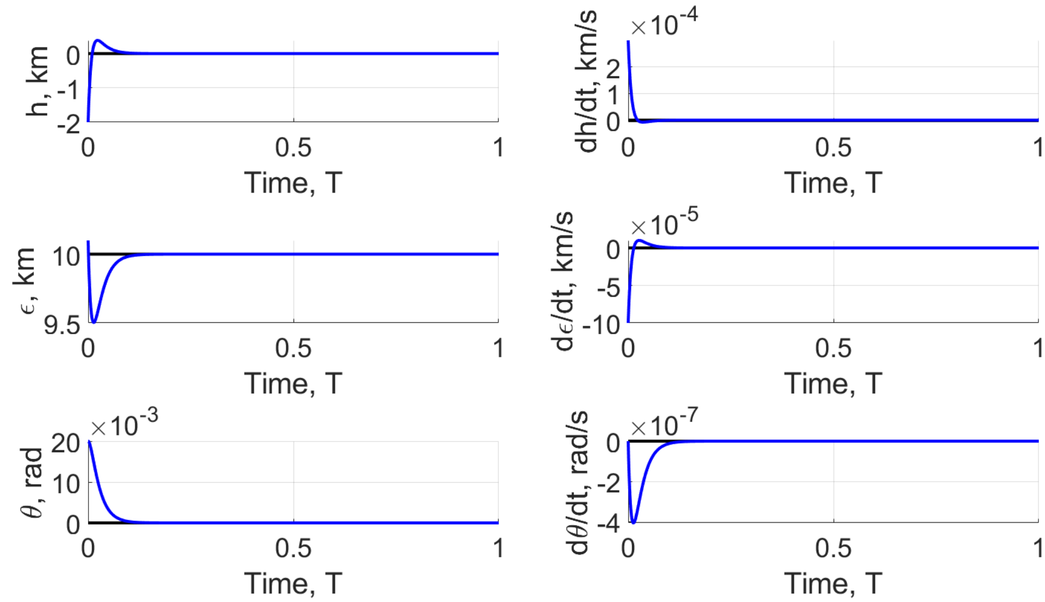

Figure 4. Coordinate state description over time for the chaser spacecraft (blue) with feedback control to track reference coordinates (black).

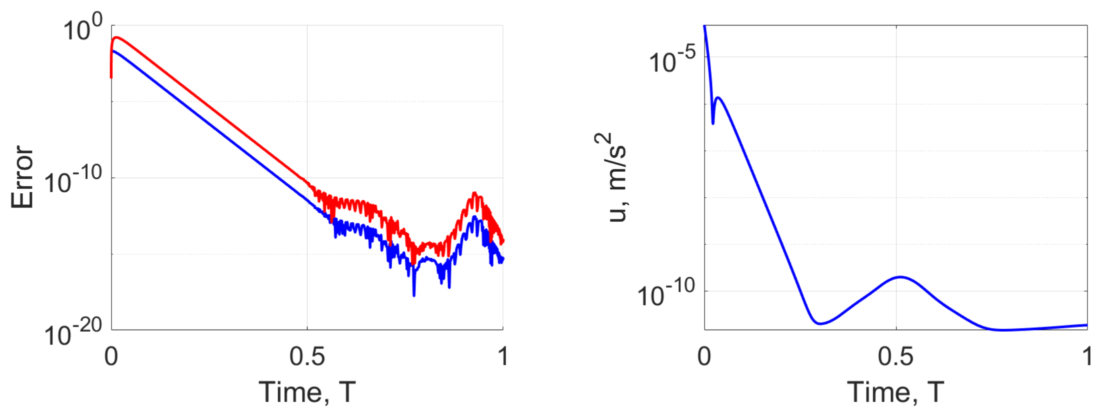

(a) Error δe (blue) and $\delta \dot{e}$ (red) magnitudes over time.

(b) Control acceleration magnitude over time.

Figure 5. Convergence analysis of the controlled chaser spacecraft trajectory.

Station-Keeping near a Sun-Earth L_1 Halo Orbit with SRP

The second simulation explores the performance of the controller in mitigating the effects of an unknown perturbing acceleration. The scenario considers two spacecraft in the Sun-Earth system that are station-keeping near a southern L_1 halo orbit. This periodic orbit is plotted relative to the Earth in the Sun-Earth rotating frame in Figure 6. The two chaser spacecraft, denoted Chaser A and Chaser B, are affected by the gravitational influence of each primary bodies as well as SRP, which is considered as a unknown disturbing acceleration in this example. The reference periodic orbit is used to define an empty formation reference point, and is unaffected by SRP. The disturbing acceleration due to SRP, $\boldsymbol{d}_{\text{SRP}}$, is defined using a cannonball model as[22]

$$\boldsymbol{d}_{\text{SRP}} = C_R \, G_1 \left(\frac{A}{m} \right) \frac{\boldsymbol{r}_{1c}}{r_{1c}^3} \tag{33}$$

where $\boldsymbol{r}_{1c}$ is the position of the chaser spacecraft with respect to the Sun. The solar radiation constant, G_1, is equal to 10^{14} kg km/s^2. Each chaser spacecraft is assumed to have an area to mass ratio of $A/m = 0.01$ m^2/kg and a reflectivity coefficient of $C_R = 0.4$, approximately consistent with a SmallSat form factor. Mass loss due to propellant usage is assumed negligible. This model serves as a proof of concept of the controller's performance in the presence of unknown perturbations. Future work will consider the capabilities of the controller in more complex formation flying scenarios in higher fidelity dynamical models.

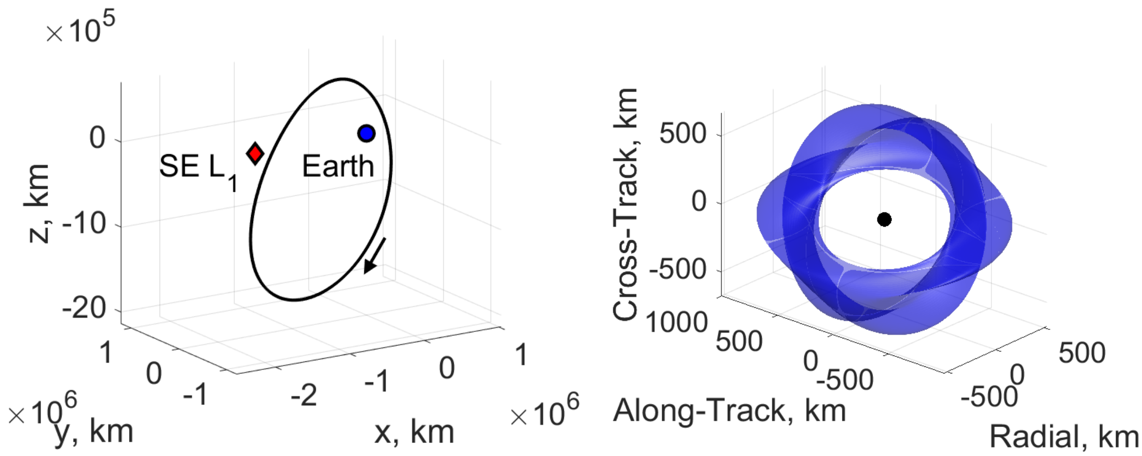

(a) A Sun-Earth L_1 halo orbit.

(b) First-order approximation of an invariant torus relative to the halo orbit.

Figure 6. Visualization of a first-order approximation of an invariant torus relative to a Sun-Earth halo orbit.

The objective of the spacecraft formation is to maintain a formation on a torus relative to the Sun-Earth halo orbit in the presence of perturbing acceleration from SRP and initial state errors. The initial state of the formation center is defined at the apogee of the halo orbit. The initial and desired geometric relative coordinates of Chaser A and Chaser B are listed in Table 2. The desired geometric coordinates of the chaser spacecraft are defined on opposite ends of the same invariant circle of the torus defined by $\varepsilon = 1000$ km. This torus is visualized in Figure 6 in the Hill frame relative to the Sun-Earth halo orbit for one revolution of the periodic orbit. Each spacecraft is controlled individually using the geometric coordinate control law to achieve the desired state relative to the empty formation center. The controller feedback gains are the same for each spacecraft and are manually tuned to achieve desired behavior. The gains are selected as $[K_1] = 1000\,[I_3]$ and $[K_2] = 100\,[I_3]$.

Table 2. Initial and desired values of the geometric relative coordinates and coordinate rates.

Quantity	Chaser A Initial Value	Chaser A Desired Value	Chaser B Initial Value	Chaser B Desired Value
h	0 km	0 km	0.5 km	0 km
ε	1000 km	1000 km	1000 km	1000 km
θ	1.5 rad	π/2 rad	-1.4 rad	$-\pi/2$ rad
$\dot{h}$	0 km/s	0 km/s	0 km/s	0 km/s
$\dot{\varepsilon}$	0 km/s	0 km/s	0 km/s	0 km/s
$\dot{\theta}$	0 rad/s	0 rad/s	0 rad/s	0 rad/s

With the dynamical model and initial conditions established, the controlled trajectories of the spacecraft are analyzed. The controlled motion of the two chaser spacecraft are propagated for one period of the halo orbit, approximately $T = 152$ days. The trajectories of the two spacecraft relative to the periodic orbit are visualized in the Hill frame in Figure 7 where the trajectory of Chaser A is represented in blue, the trajectory of Chaser B is represented in red, and the Sun-Earth halo orbit traced out by the empty formation center is represented by a black marker at the origin. The two chaser spacecraft are observed to closely follow the reference torus illustrated in Figure 6, tracing on opposite sides of the torus. However, the steady-state error caused by the SRP perturbation is evident in the relative states of the two spacecraft over time, plotted in Figure 8 using the same coloring conventions. For this example, the steady state error in h and ε is less than 1 km and error in θ is less than 0.01 rad. The perturbing effect of SRP is observed to cause almost identical positive steady-state error in h for both spacecraft, despite different initial values of h. However, steady-state error in ε is observed to have an opposite sign for each spacecraft, while additionally exhibiting oscillating error about the desired value of ε. Finally, the initial θ error for each spacecraft is minimized by the controller, and exhibits a slowly oscillating steady-state error.

The magnitude of steady-state tracking errors can be reduced via selection of larger coordinate gains, at the expense of increased cumulative control effort. For this example, the magnitude of the control acceleration of each spacecraft is plotted over time in Figure 9. Steady-state control usage is observed due to the linear approximations within the geometric coordinates definition and the presence of unknown perturbations. However, for this example, the steady-state control acceleration is again small, with an order of magnitude less than 10^{-7} m/s^2. As a comparison, for the same scenario considered without SRP acting on the chaser spacecraft, the steady-state magnitude of the control acceleration for each spacecraft is less than 10^{-9} m/s^2. Although asymptotic converge is no longer achieved in the presence of unknown perturbations, the control law demonstrates the ability to stabilize the chaser spacecraft to with small steady-state errors of the desired relative trajectory.

Formation Reconfiguration near an Earth-Moon L_2 Halo Orbit

The final simulation explores the performance of the geometric coordinate control law applied to reconfigure the chaser spacecraft relative to a target spacecraft following an Earth-Moon southern L_2 halo orbit. The response of the chaser spacecraft using the geometric control law is also compared to the response of the spacecraft using a feedback control law with error defined in terms of

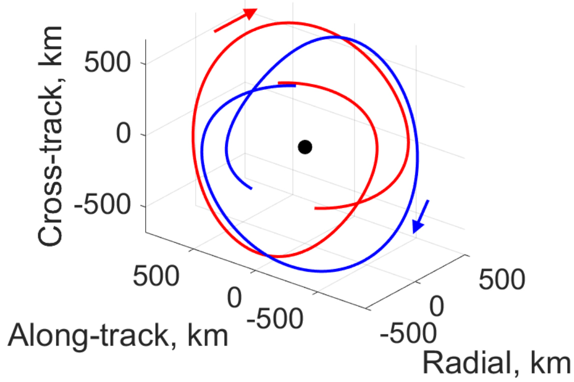

Figure 7. Controlled trajectories of Chaser A (blue) and Chaser B (red) relative to the Sun-Earth halo orbit.

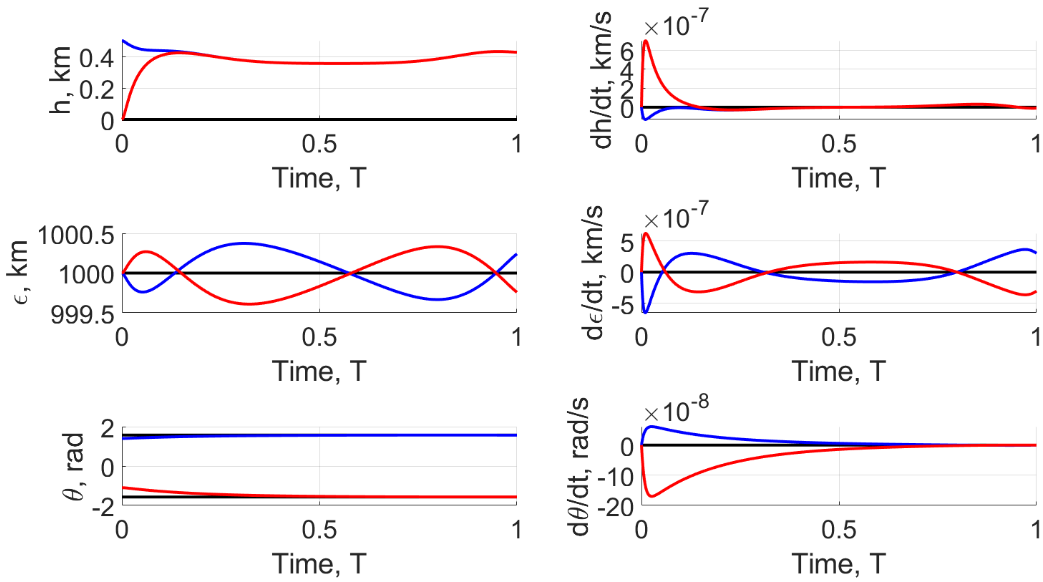

Figure 8. State description over time for the controlled trajectories of Chaser A (blue) and Chaser B (red) and the desired coordinates (black).

Cartesian Hill frame states applied to the same reconfiguration maneuver. The Cartesian control law is designed using a control Lyapunov function to be asymptotically stabilizing, and is defined as[19]

$$\boldsymbol{u} = -[K_p]\delta\boldsymbol{r} - [K_d]\delta\boldsymbol{v} - (\boldsymbol{f} - \boldsymbol{f}_d) \tag{34}$$

where $\delta\boldsymbol{r}$ is the position error and $\delta\boldsymbol{v}$ is the velocity error, both expressed in Cartesian coordinates. The matrix $[K_p]$ is a 3×3 positive definite matrix of gains on position error components, and $[K_d]$ is a 3×3 positive definite matrix of gains on velocity error components. To track a reference trajectory defined using geometric coordinates, the desired chaser coordinates are transformed into relative Cartesian state components. This transformation is then used to compute the error terms within the Cartesian control law. The relative acceleration of the chaser spacecraft, $\boldsymbol{f}$, is calculated using the nonlinear equations of relative motion defined by Eq. (4). For this example, the desired relative acceleration, $\boldsymbol{f}_d$, is the relative acceleration of a desired state along a first-order approximation of

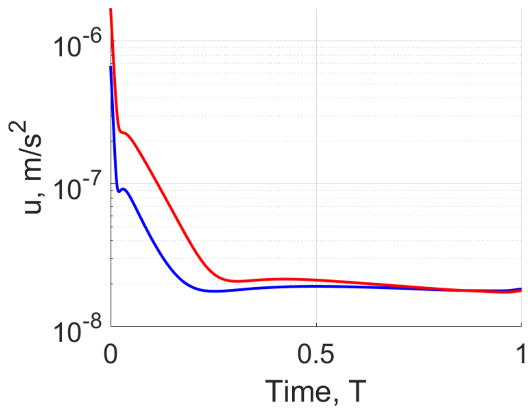

Figure 9. Control acceleration magnitude over time of Chaser A (blue) and Chaser B (red).

an invariant torus. While both control law formulations are applied to track the same trajectory, the definition of tracking errors result in different responses and corresponding trajectories.

The response of the two control laws are compared by separately integrating the chaser spacecraft using both controllers from the same formation initial conditions. The target spacecraft follows the same Earth-Moon southern L_2 halo orbit with a period of $T = 14.5$ days explored in the first example, illustrated in Figure 2(a). The chaser spacecraft is initialized on a first-order quasi-periodic orbit described by $\varepsilon = 5$ km at an initial angle of $\theta = 0$ rad. The objective of the chaser spacecraft is to apply feedback control to reconfigure its angle coordinate to $\theta = \pi/2$ rad along the torus described by $\varepsilon = 5$ km. The initial and desired values of the coordinates and coordinate rates are summarized in Table 3. The nondimensional gains for the geometric coordinate controller are selected as $[K_1] = 2000[I_3]$ and $[K_2] = 200[I_3]$. The gains for the Cartesian state controller are selected similarly as $[K_p] = 2000[I_3]$ and $[K_d] = 200[I_3]$. The controlled motion of the chaser spacecraft is propagated for one half period of the halo orbit using both control laws.

Table 3. Initial and desired geometric coordinates for the chaser spacecraft.

Quantity	Initial Value	Desired Value
h	0 km	0 km
ε	5 km	5 km
θ	0 rad	$\pi/2$ rad
$\dot{h}$	0 km/s	0 km/s
$\dot{\varepsilon}$	0 km/s	0 km/s
$\dot{\theta}$	0 rad/s	0 rad/s

Although both control laws demonstrate asymptotic convergence to the desired state, the relative trajectories produced by the two control schemes differ significantly. The trajectories produced by two control schemes are illustrated in Figure 10 where the trajectory corresponding to the geometric control law is depicted in blue and the trajectory corresponding to the Cartesian control law is depicted in red. Although the two trajectories begin at the same state and converge to the same desired trajectory, the paths exhibit distinct geometries due to the formulation of the control schemes. The state histories of the two trajectories corresponding to the two controllers are plotted over time in Figure 11, expressed using coordinates and coordinate rates using a coloring scheme consistent with Figure 8. The trajectory produced by the geometric control law is observed to maintain constant values of h and ε. This behavior is expected as from a coordinate error definition, the angle term is the only nonzero initial error term. As a result, the trajectory produced by the geometric control law traces along the torus until it converged to the desired angle.

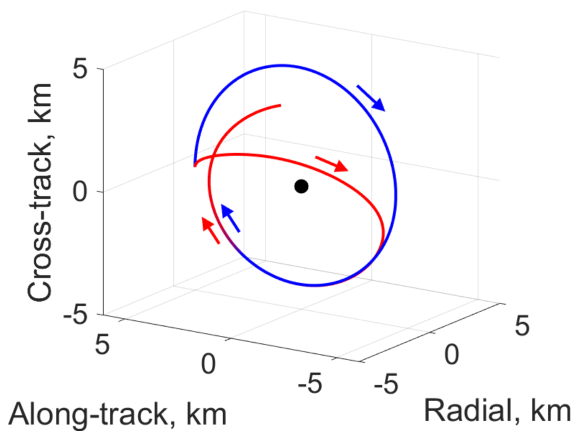

Figure 10. Trajectory of the chaser spacecraft relative to the target spacecraft using the geometric coordinate control law (blue) and Cartesian state control law (red).

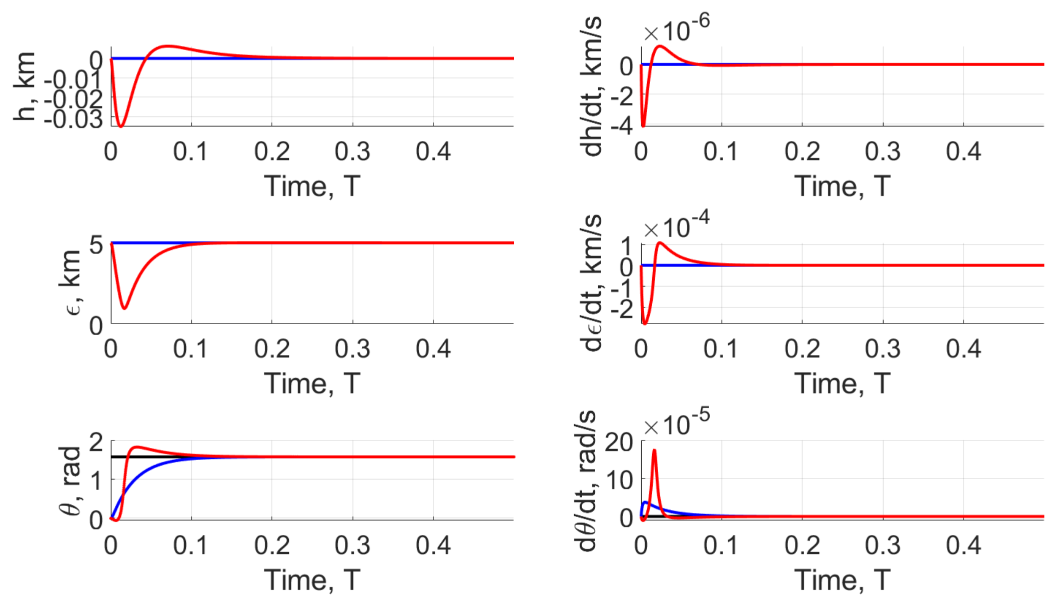

Figure 11. Coordinate and coordinate rates over time of the controlled chaser spacecraft trajectory using the geometric coordinate control law (blue) and Cartesian state control law (red).

In contrast, the trajectory produced by the control law formulated using a Cartesian state description initially departs the torus and approaches the target spacecraft before ultimately returning to the torus at the desired angle. Because of the error definition in terms of relative position and velocity expressed in the Hill frame, the trajectory produced by the Cartesian controller is not influenced by the structure of the center eigenspace during the reconfiguration maneuver. This behavior is evident in Figure 10 as the chaser spacecraft using the Cartesian controller exhibits a much closer approach to the target spacecraft than when the geometric control law is applied. Figure 12 depicts the separation distance between target spacecraft and the chaser spacecraft using the two control schemes which further illustrates a significantly different approach to the target spacecraft using the Cartesian control law. Of course, additional tuning of the Cartesian controller gains may modify these results.

The error definition and gain selection of the geometric coordinate controller provide a priori insight into the response of the chaser spacecraft relative to quasi-periodic motion. The definition of gains to correspond to the geometric of quasi-periodic tori enable stricter control on inter-spacecraft separation by selecting a larger gain on ε error relative to other gains in the $[K_1]$ matrix. The ability to circumnavigate the target spacecraft by tracing along a torus, as observed in this example, may support collision avoidance measures in spacecraft formation mission design. Additionally, the cumulative control effort required was observed to be lower for the geometric control law in this example. This result may support the future investigation of control usage optimization via the use of the geometric relative coordinate set.

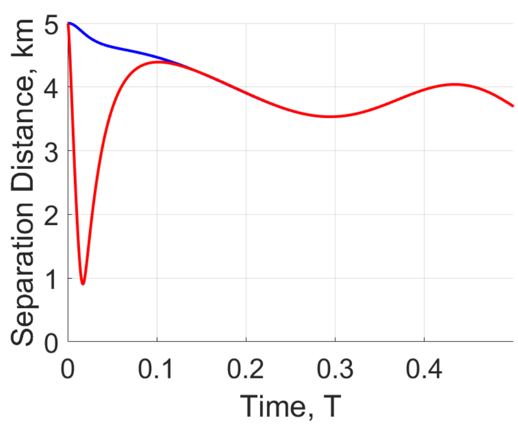

Figure 12. Separation distance over time of the chaser spacecraft from the target spacecraft using the geometric coordinate control law (blue) and Cartesian state control law (red).

CONCLUSIONS

A feedback control law is formulated using a set of geometric relative coordinates to support formation flying on quasi-periodic orbits that exist near periodic orbits in the CR3BP. The controller is valid for motion near periodic orbits that admit oscillatory modes. Differing from traditional Cartesian state control laws, the presented control law feeds back tracking errors in terms of geometry-based coordinates and coordinate rates based on quasi-periodic relation motion. This error formulation enables the straightforward definition of reference trajectories along tori and incorporation of geometric insight into gain selection. The stability of the control law is proved via a control Lyapunov function and demonstrated via numerical simulations. Asymptotic convergence to desired trajectories is observed for dynamics governed by the CR3BP and the performance of the controller is also assessed for dynamical models with unknown perturbing accelerations. Additionally, the response of the geometric coordinate based controller is compared to a feedback controller with error defined in terms of Hill frame Cartesian states. For formation reconfiguration maneuvers between states along a torus, the geometric coordinate control law demonstrates increased a priori insight into the response of the chaser spacecraft over the Cartesian control law. With the increase of spacecraft missions in three-body environments in the near-future, the ability to leverage insight into the underlying dynamical environment relative to a periodic orbit is critical for the design of efficient controller for spacecraft formations. Future applications of this work include staging orbits for rendezvous and docking operations, in-space assembly, and robotic inspection at periodic orbits.

ACKNOWLEDGMENTS

This work was supported by a Graduate Assistance in Areas of National Need Fellowship from the Smead Aerospace Engineering Sciences Department at the University of Colorado Boulder. Presentation at this conference was supported by a Beverly Sears Graduate Student Grant from the University of Colorado Boulder.

REFERENCES

[1] C. Roberts, S. Case, J. Reagoso, and C. Webster, "Early Mission Maneuver Operations for the Deep Space Climate Observatory Sun-Earth L1 Libration Point Mission," *2015 AIAA/AAS Astrodynamics Specialist Conference*, 2015.

[2] F. Renk and M. Landgraf, "Gaia: Trajectory Design with Tightening Constraints," *Proceedings of the 24th International Symposium on Space Flight Mechanics*, 2014.

[3] N. Bosanac, C. Webster, K. C. Howell, and D. C. Folta, "Trajectory Design for the Wide Field Infrared Survey Telescope Mission," *Journal of Guidance, Control, and Dynamics*, Vol. 42, No. 9, 2019, pp. 1899–1911, doi:10.2514/1.G004179.

[4] J. Gardner, J. Mather, M. Clampin, R. Doyon, M. Greenhouse, H. Hammel, J. Hutchings, P. Jakobsen, S. Lilly, K. Long, J. Lunine, M. Mccaughrean, M. Mountain, J. Nella, G. Rieke, M. Rieke, H.-W. Rix, E. Smith, G. Sonneborn, and G. Wright, "The James Webb Space Telescope," *Space Science Reviews*, Vol. 123, 02 2009, pp. 485–606, doi:10.1007/s11214-006-8315-7.

[5] B. Barden and K. Howell, "Fundamental Motions Near Collinear Libration Points and Their Transitions," *Journal of the Astronautical Sciences*, Vol. 46, 10 1998, pp. 361–378, doi:10.1007/BF03546387.

[6] E. Kolemen, N. Kasdin, and P. Gurfil, "Multiple Poincaré Sections Method for Finding the Quasiperiodic Orbits of the Restricted Three Body Problem," *Celestial Mechanics and Dynamical Astronomy*, Vol. 112, 10 2012, pp. 47–74, doi:10.1007/s10569-011-9383-x.

[7] Z. P. Olikara and D. J. Scheeres, "Numerical Methods for Computing Quasi-Periodic Orbits and their Stability in the Restricted Three-Body Problem," *Advances in the Astronautical Sciences*, 2012, pp. 911–930.

[8] N. Baresi, D. J. Scheeres, and H. Schaub, "Bounded Relative Orbits About Asteroids for Formation Flying and Applications," *Acta Astronautica*, Vol. 123, 2016, pp. 364–375, doi:10.1016.

[9] I. Elliott and N. Bosanac, "Geometric Relative Orbital Element Set for Motion Near a Periodic Orbit with Oscillatory Modes," *2020 AAS/AIAA Astrodynamics Specialist Virtual Conference*, August, 2020.

[10] B. G. Marchand and K. C. Howell, "Control Strategies for Formation Flight In the Vicinity of the Libration Points," *Journal of Guidance, Control, and Dynamics*, Vol. 28, No. 6, 2005, pp. 1210–1219, 10.2514/1.11016.

[11] L. Millard and K. Howell, "Optimal reconfiguration maneuvers for spacecraft imaging arrays in multi-body regimes," *Acta Astronautica*, Vol. 63, 12 2008, pp. 1283–1298, doi:10.1016/j.actaastro.2008.05.016.

[12] M. Bando and A. Ichikawa, "Formation Flying Along Halo Orbit of Circular-Restricted Three-Body Problem," *Journal of Guidance, Control, and Dynamics*, Vol. 38, No. 1, 2015, pp. 123–129, doi:10.2514/1.G000463.

[13] D. J. Scheeres, F.-Y. Hsiao, and N. X. Vinh, "Stabilizing Motion Relative to an Unstable Orbit: Applications to Spacecraft Formation Flight," *Journal of Guidance, Control, and Dynamics*, Vol. 26, No. 1, 2003, pp. 62–73, doi:10.2514/2.5015.

[14] L. Breger and J. P. How, "Gauss's Variational Equation-Based Dynamics and Control for Formation Flying Spacecraft," *Journal of Guidance, Control, and Dynamics*, Vol. 30, No. 2, 2007, pp. 437–448, doi:10.2514/1.22649.

[15] G. Gaias and S. D'Amico, "Impulsive Maneuvers for Formation Reconfiguration Using Relative Orbital Elements," *Journal of Guidance, Control, and Dynamics*, Vol. 38, No. 6, 2015, pp. 1036–1049, doi:10.2514/1.G000189.

[16] T. Bennett and H. Schaub, "Continuous-Time Modeling and Control Using Nonsingular Linearized Relative-Orbit Elements," *Journal of Guidance, Control, and Dynamics*, Vol. 39, No. 12, 2016, pp. 2605–2614, doi:10.2514/1.G000366.

[17] H. Khalil, *Nonlinear Systems*. Pearson Education, Prentice Hall, 2002.

[18] K. Alfriend, S. R. Vadali, P. Gurfil, J. How, and L. Breger, *Spacecraft Formation Flying: Dynamics, Control and Navigation*, Vol. 2. Elsevier, 2009.

[19] H. Schaub and J. Junkins, *Analytical Mechanics of Space Systems*. AIAA Education Series, American Institute of Aeronautics and Astronautics, Incorporated, 2014.

[20] H. Schaub, S. Vadali, J. Junkins, and K. Alfriend, "Spacecraft Formation Flying Control Using Mean Orbit Elements," *The Journal of the Astronautical Sciences*, Vol. 48, March 2000, pp. 69–87, doi:10.1007/BF03546219.

[21] V. Szebehely, *Theory of Orbits: Chapter 10 - Modifications of the Restricted Problem*. Academic Press, 1967, https://doi.org/10.1016/B978-0-12-395732-0.50016-7.

[22] J. W. McMahon and D. J. Scheeres, "Improving Space Object Catalog Maintenance Through Advances in Solar Radiation Pressure Modeling," *Journal of Guidance, Control, and Dynamics*, Vol. 38, No. 8, 2015, pp. 1366–1381, doi:10.2514/1.G000666.